

Available online at www.sciencedirect.com

SciVerse ScienceDirect

journal homepage: www.elsevier.com/locate/jmbbm

Research paper

Variability in the elastic properties of bovine dentin at multiple length scales

A.C. Deymier-Black^{a,*}, J.D. Almer^b, S.R. Stock^c, D.C. Dunand^a^a Department of Materials Science & Engineering, Northwestern University, Evanston, IL 60208, USA^b Advanced Photon Source, Argonne National Laboratory, Argonne, IL 60439, USA^c Department of Molecular Pharmacology and Biological Chemistry, Feinberg School of Medicine, Northwestern University, Chicago, IL 60611, USA

ARTICLE INFO

Article history:

Received 13 June 2011

Received in revised form

12 August 2011

Accepted 13 August 2011

Published online 24 August 2011

Keywords:

Dentin

Young's modulus

X-ray diffraction

Mineral content

Load transfer

ABSTRACT

Various methods are used to investigate the variability in elastic properties across a population of deciduous bovine incisor root dentin samples spanning different animals, incisor types, and locations within teeth. First, measurements of elastic strains by high-energy synchrotron X-ray scattering during compressive loading of dentin specimens provided the effective modulus – the ratio of applied stress to elastic phase strain – for the two main phases of dentin (hydroxyapatite crystals and mineralized collagen fibrils), shedding light on load transfer operating at the nanoscale between collagen and mineral phases. Second, Young's moduli were measured at the macroscale by ultrasonic time-of-flight measurements. Third, thermogravimetry quantified the volume fractions of hydroxyapatite, protein and water at the macroscale. Finally, micro-Computed Tomography determined spatial variations of the mineral at the sub-millimeter scale. Statistical comparison of the above properties reveals: (i) no significant differences for dentin samples taken from different animals or different incisor types but (ii) significant differences for samples taken from the cervical or apical root sections as well as from different locations between buccal and lingual edges.

© 2011 Elsevier Ltd. All rights reserved.

1. Introduction

Dentin illustrates how biological composites organize to adapt to their use and environment. Dentin makes up the bulk of teeth and acts as a shock absorber and structural support thanks to its complex composite structure (Ten Cate, 1980; Avery, 1994). Dentin is composed of three main phases: a mineral phase (hydroxyapatite, HAP), a protein phase (mostly type I collagen), and a non-load-bearing liquid phase (water, saliva or blood). The arrangement of these phases into

mineralized collagen fibrils surrounding reinforced tubules endows dentin with its exceptional mechanical properties (Ten Cate, 1980). Further, dentin consists of a hierarchy of structures; this intricacy complicates the modeling or experimental testing of its mechanical properties.

Stiffness, one of the most basic mechanical properties, is crucial to tooth performance during both elastic deformation and crack propagation (Imbeni and Kruzic et al., 2005). Kinney and Marshall et al. (2003) have shown that, as the number of experimental techniques for measuring Young's modulus

* Corresponding author. Tel.: +1 847 491 5933; fax: +1 847 491 7820.

E-mail addresses: Alixdeymier2010@u.northwestern.edu, francedanceall@yahoo.com (A.C. Deymier-Black), Almer@aps.anl.gov (J.D. Almer), S-Stock@northwestern.edu (S.R. Stock), Dunand@northwestern.edu (D.C. Dunand).

1751-6161/\$ - see front matter © 2011 Elsevier Ltd. All rights reserved.

doi:10.1016/j.jmbbm.2011.08.005

has grown, so has the range of measured values, 9 to 30 GPa in permanent human dentin. This range reflects the fact that different techniques sample different spatial scales and hence different levels of the hierarchy of structures within dentin; however, variation between individual subjects may also be important. It is therefore essential to systematically determine whether elastic properties vary spatially in dentin and, if so, what causes this variation.

A number of techniques have been used to map the Young's modulus of coronal and root dentin including micro-indentation (Kinney and Balooch et al., 1996; Meredith and Sherriff et al., 1996; Kishen and Ramamurty et al., 2000; Mahoney and Holt et al., 2000; Hosoya and Marshall, 2005), Moire interferometry (Wang and Weiner, 1998), atomic force microscopy (Balooch and Marshall et al., 2004), and tensile loading of dentin cubes removed from different locations within a tooth (Sano and Ciucchi et al., 1994). All of these studies suggest that the elastic properties of dentin vary spatially. These variations are often associated with variation in hardness and mineralization level (Wang and Weiner, 1998; Kishen and Ramamurty et al., 2000). The studies mentioned above measured the Young's modulus of dentin as an average elastic strain behavior of the HAP nano-platelets and the protein phase. Given that the HAP phase is discontinuously distributed in dentin and that dentin's modulus is much greater than that of collagen, load transfer must occur between the two phases if HAP is to reinforce the composite.

High energy X-ray scattering is well suited for the measurement of strains within the individual components of biomineralized composites such as bone and dentin. This method has been used to determine *in situ* the strain behaviors of HAP and the collagen fibrils in bovine (Gupta and Wagermaier et al., 2005; Gupta and Seto et al., 2006; Gupta and Wagermaier et al., 2006; Akhtar and Daymond et al., 2008a,b), rat (Stock and Yuan et al., 2011), and canine (Almer and Stock, 2005, 2007) bone (under compressive (Almer and Stock, 2005, 2007; Akhtar and Daymond et al., 2008a,b; Stock and Yuan et al., 2011) and tensile (Gupta and Wagermaier et al., 2005; Gupta and Seto et al., 2006; Gupta and Wagermaier et al., 2006) loading conditions), fallow deer antler (Akhtar and Daymond et al., 2008a,b), and bovine tooth (Almer and Stock, 2010; Deymier-Black and Almer et al., 2010, 2011). In the case of bovine dentin, load transfer between the collagen and the HAP has been investigated at ambient temperature during monotonic loading (Deymier-Black and Almer et al., 2010) and as a function of freezing cycles (Deymier-Black and Almer et al., 2011). The latter two studies show that, under compressive elastic loading, stress is transferred to the HAP at a level exceeding that predicted by simple load-transfer composite models and that this behavior is not affected by prior freezing.

These two studies (Deymier-Black and Almer et al., 2010, 2011) provided the first basic information about load transfer mechanisms in bovine dentin, but did not focus on how the elastic modulus varies between different teeth and different animals, how the volume fraction of different phases within the dentin vary with location, or how repeatable measurements are of the phase elastic behavior. Quantifying the level of repeatability of a measurement method is essential to assessing whether observed differences have

physical significance. Spatial inhomogeneities in Young's modulus affect properties such as fatigue limit, load transfer, and fracture toughness, and if present, must be incorporated into numerical models so they can accurately predict these properties.

The present study of bovine root dentin utilizes multiple techniques to determine how elastic properties (at the nanoscale, phase level and at the macroscale dentin level) vary within and between bovine incisors. Fibrillar and HAP apparent moduli (defined as the bulk applied stress, σ_{app} , divided by the phase strain, e^i , and reflecting the elastic behavior of a phase within the composite) are measured by synchrotron high-energy X-ray scattering and used to investigate how load transfer between the phases of dentin varies with location within dentin. Micro-computed tomography (μ CT) is used to measure submillimeter-scale variations of mineral levels within the volumes probed by X-ray scattering. Average macroscopic dentin Young's moduli are determined from ultrasonic velocity measurements. Finally, the volume fractions of the three phases of dentin are measured at the macroscopic level through thermogravimetric analysis (TGA) to determine the relationship between average mineralization levels and elastic properties. Further, correlation statistics were calculated for all of the measured values.

2. Materials and methods

2.1. Dentin samples

Erupted deciduous bovine incisors were extracted from five mandibles (labeled as J1–J5) from cows of the Black Angus breed, ~18 months in age. The jaws were obtained less than one hour after slaughter from the Aurora Packing Co (North Aurora, IL) and maintained at ambient temperature (~25 °C) during transport (1.5 h). As the first incisors were damaged, only the second and third incisors were removed from each of the jaws using scalpels and dental tools. The fourth incisors were only removed from J5. Second incisors from the left and right side of the jaw were extracted from all five jaws. Left and right third incisors were removed from all five jaws except for J1 in which the third left incisor was damaged. Upon removal, these 21 incisors were immediately placed in a solution of phosphate buffered saline (PBS) and frozen at –20 °C.

A few days after extraction, the teeth were thawed to room temperature and cut into specimens for mechanical testing. The incisor was clamped at the crown to avoid damage to the root and cut perpendicular to the long root axis using a Buehler Isomet-1000 precision diamond wafering saw. A first cut was made 5–10 mm from the root apical tip (i.e., the end farthest from the crown) and a second, parallel cut was made 8 mm higher to create a specimen. If the size of the incisor allowed, a third, parallel cut was made 8 mm above the second cut to create a second cervical specimen, from the region below the enamel-cementum junction (gum line). The incisors were constantly hydrated with either PBS during mounting or deionized water during cutting. In most cases, two quasi-cylindrical dentin samples with a height of ~7.5 mm, an average buccal–lingual axis of ~6 mm and an

Table 1 – Classification of the samples according to animal (jaw), type of tooth, and location within the tooth (cervical or apical root section).

Location	Incisor	Jaw				
		1	2	3	4	5
Cervical	2nd	1_2R2	2_2R2	3_2R2	4_2R2	5_2R2
		1_2L2	2_2L2	3_2L2	4_2L2	5_2L2
	3rd	1_2R3	2_2R3	3_2R3	4_2R3	5_2L3
			2_2L3	3_2L3	4_2L3	
	4th					5_2R4
						5_2L4
Apical	2nd	1_1R2	2_1R2	3_1R2	4_1R2	5_1R2
			2_1L2		4_1L2	5_1L2
	3rd					5_1R3
						5_1L3
	4th					5_1R4
						5_1L4

average mesial–distal axis of ~4 mm were obtained for each incisor.

Due to some incisor damage, a total of 32 usable samples resulted (Table 1). The naming convention for the samples is: (i) the number of the jaw from which the sample was extracted, (ii) an underscore followed by apical or cervical root section represented by the numbers 1 or 2, respectively, followed by (iii) R or L for right or left side of the jaw, (iv) the type of incisors (2, 3, or 4). After cutting, the samples were immersed in PBS and refrozen at –20 °C until X-ray scattering experiments could be performed.

2.2. X-ray scattering experiments

High-energy X-ray scattering was performed at beamline 1-ID-C of the Advanced Photon Source (APS) at Argonne National Laboratory (Argonne, IL, USA) and followed procedures used previously for bovine dentin (Deymier-Black and Almer et al., 2010, 2011). Throughout the experiments, the samples were hydrated with PBS at ambient temperature. Uniaxial compressive loading of the dentin cylinders was carried out using a MTS 858 load frame with a customized base and hydraulic loading. The samples were loaded in increments of 20 MPa from 0 to 80 MPa, in the elastic range of human dentin (Craig and Peyton, 1958) and just above the apparent yield point of bovine dentin (Sano and Ciucchi et al., 1994). A 15 kN load cell measured the force on the sample with a precision of approximately 15 N (0.1%). Macroscopic strain was calculated from the recorded cross-head displacement corrected for machine compliance.

Wide angle X-ray scattering (WAXS) and small angle X-ray scattering (SAXS) measurements were taken at 8–10 locations along the buccal–lingual direction of the incisor depending on the sample size, as illustrated in Fig. 1. The sampling locations were 0.5 mm apart (positions A–J) and located at the vertical center of the dentin samples. The monochromatic 65 keV X-ray beam was 35 μm wide, vertically focused to 30 μm, providing a ca. twentyfold flux density increase as compared to the unfocused beam, and extended through the thickness of the dentin, thus sampling a volume of ~0.004 mm³. The HAP and fibrillar strains in dentin were averages for these

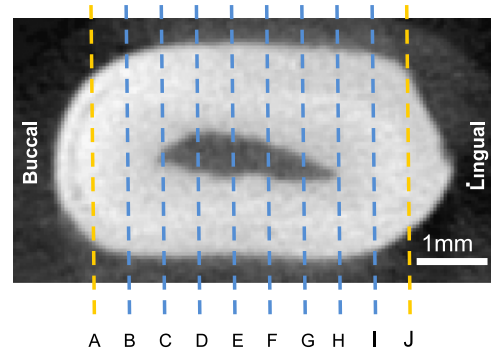


Fig. 1 – Micro-computed tomography image of a dentin sample cross-section. Dotted lines represent the X-ray beams (width to scale) penetrating through the samples.

small volumes and therefore included both intertubular and peritubular dentin.

The WAXS diffraction patterns from the crystalline HAP nanoplatelets were recorded using a MAR165 Single Chip CCD Detector System (MarUSA, Inc., Evanston, IL) (diameter of 165 mm) placed 698 mm from each specimen. The SAXS patterns produced by the regularly spaced HAP crystals in the mineralized collagen fibrils in dentin, were recorded using a Bruker6500 CCD camera (Bruker AXS, Inc., Madison, WI) at a sample-to-camera distance of 4000 mm. To obtain the SAXS pattern, the MAR165 detector was translated out of the X-ray beam thus exposing the Bruker CCD camera. The X-ray exposure times were 15 s per WAXS and 5 s per SAXS pattern, except those taken from J5 which had a WAXS exposure time of 10 s. A disk of pressed ceria powder (CeO₂, NIST Standard Reference Material SRM-674a), which was inserted before and after the loading experiments, was used as a standard.

Taking into account the beam flux, size, and energy, the sample density, and the exposure times (Appendix), each sampled location was subjected to a dose of 34 kGy per WAXS/SAXS combined measurement at a given stress level, with samples from J5 receiving 28 kGy per measurement. Since each location was measured at five different applied stresses, the total dose per location was 170 kGy for all samples (140 kGy for J5). Although doses at this level affect the fracture properties of bone samples (Currey and Foreman et al., 1997; Nguyen and Morgan et al., 2007; Barth and Launey et al., 2010), previous research has indicated that these doses have no measurable effect on the elastic properties of bovine dentin (Currey and Foreman et al., 1997; Singhal and Deymier-Black et al., 2011).

2.3. X-ray scattering analysis

To determine HAP lattice spacing, from which elastic strain can be calculated, procedures were followed similar to those presented elsewhere (Wanner and Dunand, 2000; Young and Almer et al., 2003; Daymond and Young et al., 2007; Young and Almer et al., 2007; Young and DeFouw et al., 2007). First, the beam center, detector tilt, and sample-to-camera distance for the MAR detector were determined with the program Fit2D (Hammersley, 1997, 1998) using the CeO₂ 200 and CeO₂ 333 reflections of the ceria standard. These calibration parameters were then used to convert the sample diffraction

patterns from polar to Cartesian coordinates. A MATLAB (MathWorks, Inc., Natick, MA) algorithm then fitted the specific crystallographic reflections (HAP 00.2, HAP 22.2, and HAP 00.4) used by (Almer and Stock, 2005, 2007). The radial peak profile was fit using a pseudo-Voigt function to find the average center of the peak intensity (R) at each azimuthal angular position (η). Using calibration parameters and the X-ray wavelength, R was then converted into a d-spacing. To obtain a HAP lattice strain, the stress-free point (R_0) was determined by plotting R vs. $\sin^2(\Psi)$, where $\Psi = \eta\theta \cos(\eta)$ and θ is the Bragg angle, for all stresses and determining the point of intersection of the curves. The internal lattice strain of a specific HAP reflection in the dentin can then be determined as $\varepsilon(\eta) = (R_0 - R(\eta))/R(\eta)$. The best-fit curve to $\varepsilon(\eta)$ vs. η allows the axial and transverse strain components $e_{11} = \varepsilon(90^\circ \pm 10^\circ, 270^\circ \pm 10^\circ)$ and $e_{22} = \varepsilon(180^\circ \pm 10^\circ, 360^\circ \pm 10^\circ)$, respectively, to be found using equations for two-dimensional detectors (He and Smith, 1998).

Fit2D calibration parameters calculated from the SAXS diffraction patterns were used to calculate the fibrillar strain. The radial peak center, R , of the third-order mineralized fibril peak was fit over the azimuthal ranges of $90 \pm 30^\circ$ and $270 \pm 30^\circ$, and was then converted to a D-period, associated with the regular spacing of HAP platelets along the collagen fibril axes, using the previously described calibration parameters. For the case of the fibrils, the strain-free D-period, or radial peak center, R_0 , was assumed to be equal to the value measured when no stress was applied to the sample. Similarly to the WAXS measurements, the longitudinal strain of the fibril, $e_{11}^{fib} = \varepsilon(90^\circ \pm 30^\circ, 270^\circ \pm 30^\circ)$, was calculated with a best-fit curve of $\varepsilon(\eta) = (R_0 - R(\eta))/R(\eta)$ vs. η . Due to low signal and scattering interference in the direction transverse to the loading axis, the strain $e_{22}^{fib} = \varepsilon(0^\circ \pm 10^\circ, 180^\circ \pm 10^\circ)$ was not calculated. After the scattering measurements, the samples were placed in PBS and frozen at -20°C .

2.4. Micro-computed tomography for cross-sectional area determination

Cross-sectional areas of the dentin samples were acquired using μCT in order to accurately calculate the applied stress. Before performing μCT , the samples were thawed and placed in a sample holder filled with room temperature PBS. The cross-sectional areas of the samples were measured using laboratory μCT (MicroCT 40, Scanco Medical, Southeastern, PA, USA). The microfocus X-ray tube was operated at 70 kV and 114 μA , and the beam passed through a 0.13 mm thick Be window on the X-ray tube and through a 0.50 mm thick Al filter before encountering the sample. With this system, 20 slices were collected with a 0.300 s integration time for each projection. Reconstruction was done on a 1024×1024 grid with 30.7 μm voxels (volume elements). Dentin cross-sectional area was determined using a threshold corresponding to 1.6 cm^{-1} , a value typically employed in the μCT lab for cortical bone at this tube voltage. Visual inspection revealed that this threshold faithfully reproduced the samples' cross-sections. The maximum uncertainty on the cross-sectional area of the samples considering a large threshold error of 0.5 pixels in every direction is $\sim 4.3\%$. In reality the uncertainty on the area is significantly less than this value (Stock, 2009).

The applied stress, σ_{app} , was calculated from the ratio of the applied force as measured by the load cell to the μCT

determined cross-sectional area. The maximum uncertainty on the applied stress is $\sim 4.3\%$.

2.5. Ultrasonic Young's modulus measurements

Ultrasonic measurements were used to determine the Young's modulus of the dentin samples after the scattering experiments. Two pairs of 5 MHz transducers, one for longitudinal and one for shear waves, were used to transmit and collect a pulse of ultrasound across the entire cross-section of the dentin samples. The ultrasonic instrument was initially zeroed by making direct contact between the faces of the two transducers and measuring the time, t_0 , required for the ultrasonic pulse to travel from one transducer to the next. Calibration was then conducted with single-crystal copper samples along the 100, 110 and 111 directions. The longitudinal transducers were then placed on either side of the long axis of the dentin sample so that their faces were in contact with its flat and parallel surfaces. The ultrasonic pulse was sent through the sample and the time of travel, t_ℓ , was measured. Once the longitudinal data were acquired, the shear transducers were used and the above process was repeated to obtain the shear time of travel, t_s . The longitudinal and shear measurements were performed three times on each sample to improve precision ($\sim 6\%$ precision). By dividing the average values of t_ℓ and t_s from the three measurements by the sample height (measured with point calipers at three different locations), longitudinal and shear sound velocities, V_ℓ and V_s , were determined. Assuming the material is isotropic, these sound velocities were used to solve for the sample's Poisson's ratio (ν) and Young's modulus (E) via:

$$V_s = \sqrt{\frac{E}{2\rho(1+\nu)}} \quad (1a)$$

$$V_\ell = \sqrt{\frac{E}{\rho(1+\nu)(1-2\nu)}} \quad (1b)$$

where $\rho = 1.96 \pm 0.04 \text{ g/cm}^3$ is the average dentin density, determined by the Archimedes method in water for all samples from J5. The isotropic assumption is reasonable as anisotropy in human dentin, which is similar to bovine dentin, is minimal ($<10\%$) (Kinney and Gladden et al., 2004).

2.6. Thermogravimetry

To determine the weight fractions of HAP, collagen and water in all studied samples, TGA was performed as described previously (Deymier-Black and Almer et al., 2010). After X-ray and ultrasonic measurements, each dentin cylinder was cut into three disks perpendicular to the sample long axis with the diamond saw described above. The central disk had a thickness of 1 mm and a midline located at the same height as the scattering measurements. This disk was then further cut into four $\sim 10 \text{ mg}$ pieces at the buccal, lingual, mesial and distal sides of the incisor. TGA measurements were performed on the small specimens cut from the mesial or distal edges of each sample using a Mettler Toledo TGA/SDTA 851 Thermogravimetric analyzer with a $\pm 1 \mu\text{g}$ precision. The samples were kept in PBS until immediately preceding

Table 2 – Table of the uncertainties for strain and apparent moduli. Uncertainties in the strain are calculated as the standard deviation of the measured strains from the singular value decomposition fit assuming a normal distribution. Apparent modulus uncertainties are standard deviations from the best fit line assuming a normal distribution. Uncertainties for the apparent moduli within samples, between samples, and between jaws are average standard deviations from the measured mean values.

Uncertainties:	Strain ($\mu\epsilon$)	Apparent modulus (GPa)	Within samples (GPa)	Between samples (GPa)	Between jaws (GPa)
WAXS	207	7.2	6.2	3.4	1.01
SAXS	1069	5.8	4.3	2.7	1.5

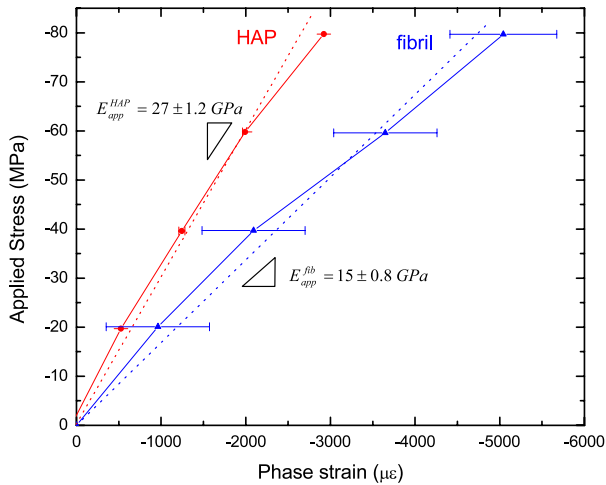


Fig. 2 – Representative plot of HAP and fibrillar elastic strain as a function of applied stress for sample 3_2R2, location E. The slopes of the two best-fit lines are the apparent moduli $E_{app}^{HAP} = 27 \pm 1.2$ GPa and $E_{app}^{fib} = 15 \pm 0.8$ GPa.

the measurement when they were blotted dry and placed in an alumina pan. Each sample was heated in air from 20 to 650 °C at a rate of 10 °C/min and maintained at the maximum temperature for 5 min. Weight fractions of water and collagen were determined from the accumulated weight loss at plateaus located between 20 and 200 °C and between 200 and 500 °C, respectively, according to Holager (1970). Literature values of collagen and HAP density, 1.34 and 3.16 g/cm³ respectively (Fels, 1964; Gaines and Skinner et al., 1997), were then used to convert weight fractions to volume fractions.

2.7. Micro-computed tomography for localized mineral content determination

The top dentin disk removed from sample 2_2L3 during sample preparation for TGA was examined after dehydration in progressively higher concentrations of ethanol solutions (25, 50, 75 and 100% ethanol) using the Scanco Medical MicroCT 40 system as described above, except that the tube was operated at 45 kV and 177 μ A. The dehydrated sample was placed in a 12.3 mm diameter sample holder. A single slice, located as close as possible to the cross-section sampled by X-ray scattering was reconstructed with 6 μ m voxels.

Average linear attenuation coefficients were obtained for the eight synchrotron sampling volumes (parallelepipeds

measuring 35 × 30 μ m × sample thickness) in the original dentin sample. These linear attenuation coefficients were then converted to HAP mineral content by comparison with the Scanco calibration phantom composed of varying HAP concentrations: 0.0997, 0.2000, 0.4012, and 0.7994 g/cm³ of HAP.

2.8. Statistical analysis

Errors on the HAP and fibrillar strains were calculated as the standard deviation of the measured strains from the singular value decomposition fit assuming a normal distribution (He and Smith, 1998). All linear slopes of the HAP and fibrillar strain as a function of applied stress were fit using the least-squares method to obtain a best fit line. Errors on the reported slopes are standard deviations assuming a normal distribution. All uncertainties are reported in Table 2.

Significant differences in the means of the HAP and fibrillar apparent moduli for different populations were measured at a significance level of $p < 0.05$ by one-way ANOVA (ANalysis Of VAriance) using Origin 7 (Origin Lab, Northampton, MA, USA). For situations where significant differences were measured, multiple t-tests (also $p < 0.05$) determined which of the population means differed.

3. Results

Values of e_{11}^{HAP} , e_{22}^{HAP} and e_{11}^{fib} from the scattering analysis vary linearly as a function of applied stress for all of the samples tested here. Apparent moduli, $E_{app}^i = \frac{\sigma_{app}}{e_{11}^i}$, of phase i (HAP or fibril) was calculated by linear regression; a representative plot of phase strain as a function of stress for a single location on a single sample is shown in Fig. 2. For this sample, $E_{app}^{HAP} = 27 \pm 2.7$ GPa and $E_{app}^{fib} = 15 \pm 1.8$ GPa (mean \pm standard deviation).

Out of the 8–10 locations (see Fig. 1) measured for each sample with X-ray scattering, the first and last (A and J) were not used due to insufficient thickness of the sample resulting in poor scattering statistics (Deymier-Black and Almer et al., 2011). Fig. 3 shows the mean apparent modulus values, for each of the dentin samples, calculated from the average of the 6–8 measured locations. The values are plotted from lowest (left) to highest (right) HAP volume fraction as determined from TGA. The average intra-sample standard deviation for apparent elastic modulus across the eight locations in each sample is 6.2 GPa for HAP and 4.3 GPa for the fibrils. These values are significantly higher than the inter-sample standard deviations calculated between the average apparent elastic moduli measured for each sample which are 3.4 GPa for HAP and 2.7 GPa for the fibrils (Table 2). By averaging the

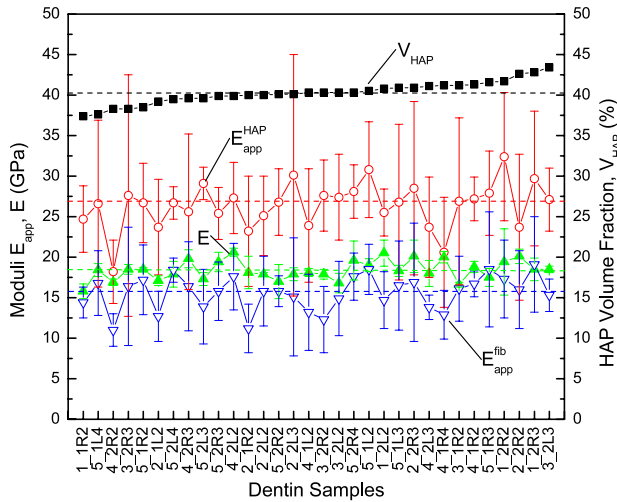


Fig. 3 – Plot of experimentally measured properties: HAP volume fraction (■), HAP apparent modulus (○), fibrillar apparent modulus (△) and ultrasonic Young's modulus (◆) for all of the samples. For the apparent moduli, each point is the average of the 6–8 measured locations in the sample. Overall average values are represented by dotted lines.

slopes from all of the 6–8 locations from all of the 32 samples (254 slopes per phase), the overall average HAP and fibrillar apparent elastic moduli were calculated to be 26.5 ± 7.2 GPa and 16.1 ± 4.9 GPa, respectively (dotted lines in Fig. 3). The relatively large standard deviations reflect positional variations within individual samples instead of variations between samples. Ultrasound average Young's modulus of the 32 dentin samples was 18.0 ± 1.2 GPa (Fig. 3).

The thermogravimetric analysis provided a measure of the water, protein and mineral content of bovine dentin. The average HAP volume fraction among all the samples was $40.3 \pm 1.4\%$, while those for collagen and water were $31.5 \pm 1.0\%$ and $28.2 \pm 2.2\%$, respectively.

3.1. Variation between animals

The average apparent HAP moduli between the five animals varied from 25.4 ± 8.2 GPa for J1 and 27.8 ± 6.7 GPa for J5. The fibrillar apparent moduli varied from 13.7 ± 6.3 GPa for J2 to 17.6 ± 4.4 GPa for J5. One-way ANOVA testing showed that although there was no significant difference in apparent HAP moduli between animals, there was a significant difference for the fibrillar moduli. No significant difference in the ultrasonic modulus or TGA sample composition was found between samples from the different animals.

3.2. Variation between different incisors

The apparent HAP moduli for the second, third, or fourth incisors across the five animals were 26.7 ± 6.3 , 26.8 ± 8.4 , and 29.1 ± 6.8 GPa, respectively; for the fibrils they were 16.2 ± 4.5 , 16.4 ± 5.1 and 17.6 ± 4.0 , respectively. One-way ANOVA showed no significant difference in HAP or fibril apparent moduli for second, third, or fourth incisor populations. Similarly, both ultrasonic moduli and phase volume fractions showed no significant variations between the three incisors.

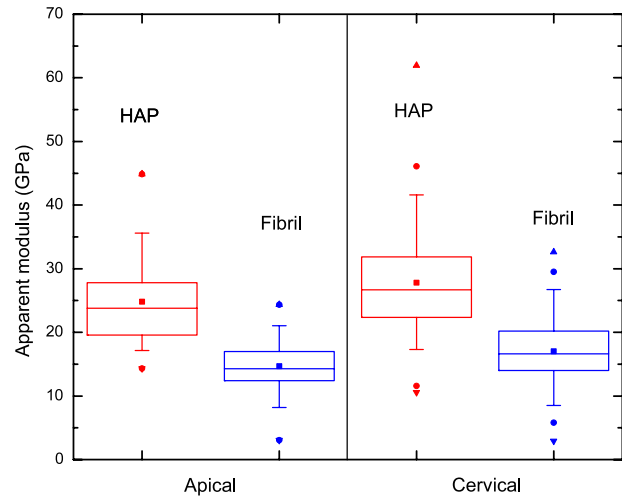


Fig. 4 – Box plots showing the mean (■), maximum and minimum values (▲ ▼), as well as the 99th and 1st (●), 95th and 5th (whiskers), and 75th, 50th, and 25th percentiles (box) for HAP and collagen apparent moduli for the entire populations of samples taken from the apical and cervical root sections. The cervical root population consists of 20 samples while the apical root population consists of 12 samples.

3.3. Spatial variations within a single incisor

The average apparent modulus values for apical root section samples were 25.7 ± 6.5 GPa for HAP and 15.2 ± 3.9 GPa for the fibrils versus 28.9 ± 7.6 GPa and 17.6 ± 5.3 GPa, respectively, for the cervical root sections. T-tests indicated that both the HAP and the fibrillar apparent moduli were significantly less for the apical samples as compared to the cervical samples (Fig. 4). When comparing cervical and apical root sample populations, no statistically significant differences were found for the ultrasonic modulus or the volume fractions of HAP, collagen, or water.

The average apparent modulus for the location near the buccal edge (B) was 26.6 ± 8.4 GPa for HAP and 13.4 ± 6.1 GPa for the fibril, while the values for the location nearest the lingual edge (I) were 32.0 ± 10.0 GPa for HAP and 18.3 ± 5.2 GPa for the fibril. One-way ANOVA tests showed a statistically significant difference in HAP apparent elastic modulus as well as fibrillar apparent modulus at different locations across the incisor. Although no two neighboring locations (e.g., B and C, or G and H) ever had statistically different apparent modulus values, the locations farthest from each other, i.e., the volume on the buccal edge (B) compared to the volume at the lingual edge (I), were significantly different. T-tests revealed that volumes near the buccal edge of the dentin samples had significantly smaller apparent moduli for both the HAP and the fibrils than the locations on the lingual edge (Fig. 5).

3.4. Correlations

Although the ultrasonic modulus and sample compositions did not differ significantly with incisor type, location in the tooth, or animal (jaw), these values correlated both with each other and with those calculated from the synchrotron

Table 3 – Table showing correlation coefficients, R, and p-values (in parentheses) between all of the measured values. Bold $p < 0.05$, Bold and italicized $0.05 < p < 0.1$, for the remaining values $p > 0.1$.

	HAP content	Collagen content	Water content	HAP apparent modulus	Fibril apparent modulus	Ultrasonic modulus
	Vol fraction	Vol fraction	Vol fraction	GPa	GPa	GPa
HAP content	1					
Collagen content	0.72 (<0.0001)	1				
Water content	-0.95 (<0.0001)	-0.90 (<0.0001)	1			
HAP apparent modulus	0.25 (0.17)	0.00 (0.99)	-0.16 (0.39)	1		
Fibril apparent modulus	0.23 (0.20)	-0.12 (0.51)	-0.09 (0.61)	0.68 (<0.0001)	1	
Ultrasonic modulus	0.34 (0.05)	0.03 (0.87)	-0.21 (0.24)	0.12 (0.51)	0.32 (0.07)	1

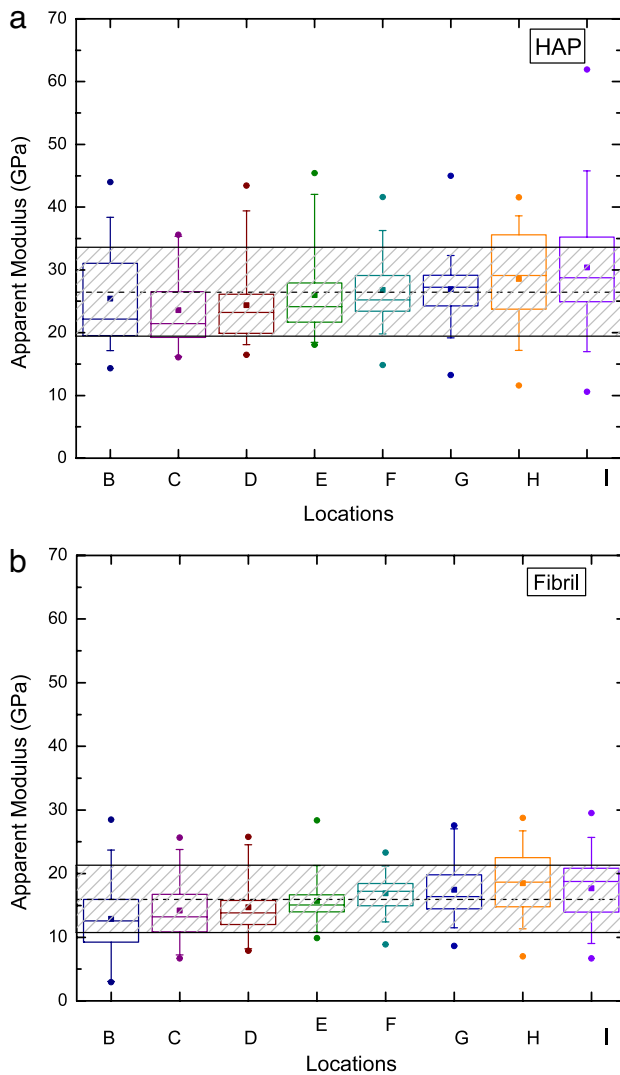


Fig. 5 – Box plots showing the mean (■), the 99th and 1st (●), 95th and 5th (whiskers), and 75th, 50th, and 25th percentiles (box) for (A) HAP and (B) fibrillar apparent moduli for the entire populations of samples at different X-ray measurement locations. Each box plot represents data taken from all 32 samples except locations H and I which represent 31 samples each due to one sample having only six measurable locations instead of eight.

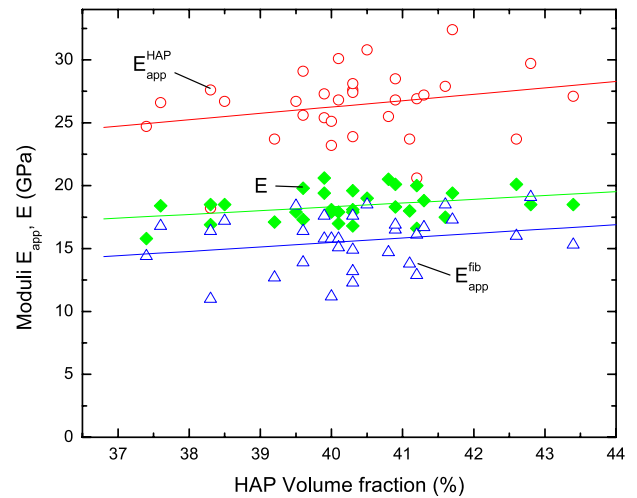


Fig. 6 – Plot of the ultrasonic modulus (◆) and HAP (○) and fibrillar (△) apparent moduli as a function of HAP content as determined from thermogravimetric analysis.

analysis (Table 3). The strongest correlations were between the volume fractions of the three dentin phases. The collagen and HAP fractions were positively correlated to each other ($R = 0.715$) and were both negatively correlated with water content ($R = -0.898$ and -0.946 , respectively). It is well established that the volume fractions of reinforcement and matrix of a composite such as dentin affects the mechanical and load transfer properties (Kinney and Marshall et al., 2003). However, the water and collagen contents had no statistically significant effect ($p > 0.05$) on either the ultrasonic, HAP or fibrillar moduli. The HAP content, on the other hand, was positively correlated with the ultrasonic modulus ($R = 0.3438$). Although the correlations were not statistically significant ($p = 0.172$ and 0.204), the HAP and fibrillar moduli were also positively correlated with HAP content with $R = 0.248$ and 0.231 , respectively (Fig. 6). These moduli were also correlated to each other. The ultrasonic and fibrillar moduli were positively correlated ($R = 0.318$) as were the HAP and fibrillar moduli ($R = 0.678$).

At the eight different locations within sample 2_2L3, μ CT measured mineral contents between 1070 to 1289 mg/cm^3 (i.e., HAP volume fractions of 33.9 to 40.8%). The average μ CT-determined HAP volume fraction of $35.7 \pm 2.9\%$ was smaller than the TGA-obtained value of 43.2% for sample 2_2L3, in a more apical volume of the root dentin. Fig. 7 compares μ CT

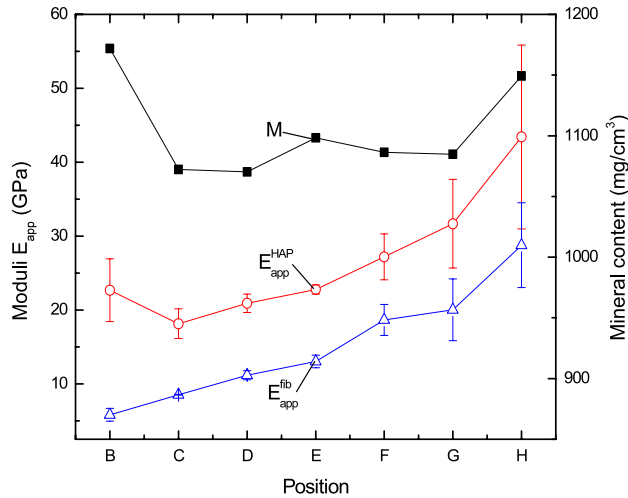


Fig. 7 – Plot of the HAP (○) and fibrillar (△) apparent moduli as well as the mineral content as determined from micro-computed tomography (■) as a function of location in sample 2_2L3. Scatter bars on the apparent moduli are standard deviations assuming a normal distribution.

derived mineral level with scattering derived moduli. When the location dependent mineral contents were compared with the apparent moduli measured at these same eight locations, a correlation coefficient of $R = 0.855$ was obtained.

4. Discussion

4.1. Comparison with literature data and models

The average values of apparent elastic moduli for the HAP (26.5 ± 7.2 GPa) and the fibrils (16.1 ± 4.9 GPa) agree with previous X-ray scattering measurements performed on similar bovine dentin samples. A first article reported a HAP apparent modulus of 18 ± 2.0 GPa for a single sample (near the lower bound of the present distribution) (Deymier-Black and Almer et al., 2010) while a later study reported a HAP apparent modulus of 26 ± 8.0 GPa for 12 samples (Deymier-Black and Almer et al., 2011) and a fibrillar apparent modulus of 16 ± 5.5 GPa for the same 12 samples (Deymier-Black and Almer et al., 2011).

The value of 18 ± 1.2 GPa for the Young's modulus determined by ultrasonic measurements is slightly lower than previously reported ultrasonic measurements. For bovine dentin from animals of an unspecified age, one study reports a modulus of 21 GPa (no standard deviation reported) (Gilmore and Pollack et al., 1969). For permanent human dentin, the ultrasonic modulus is 24.4 GPa (with <1.2 GPa standard deviation) (Kinney and Gladden et al., 2004). The lower value found here may be caused by the deciduous nature of the dentin samples which may have decreased stiffness (Avery, 1994). It may also result from increased acoustic scattering or sample size effects (Talmant and Foiret et al., 2011) which could decrease the value up to 10%.

The average volume fractions of HAP, collagen and water in the present bovine dentin samples (40.3 ± 1.4 , 31.5 ± 1.0

and $28.2 \pm 2.2\%$, respectively) differs slightly from prior TGA-derived values for bovine permanent dentin ($44.6 \pm 0.6\%$ for HAP, $33.2 \pm 0.2\%$ for collagen and $22.2 \pm 0.2\%$ for water) (Sakae and Mishima et al., 1988). This increase in water content and decrease in HAP content may be due to the fact that the present study investigated deciduous teeth which are known to have decreased dentin hardness (Avery, 1994) often associated with lower mineral content.

Known volume fractions of HAP, collagen and water and Young's moduli for these phases allow calculation of a lower bound for the apparent elastic modulus of HAP, E_{HAP}^{app} . This limit, which corresponds to an upper bound for the HAP elastic strain (and thus HAP stress for a given composite strain) is given by the Voigt composite model (Currey, 2002):

$$E_{HAP}^{app} = E_{HAP}V_{HAP} + E_{col}V_{col} + E_{H_2O}V_{H_2O} \quad (2)$$

where $E_{HAP} = 114$ GPa (Gilmore and Katz, 1982), $E_{col} = 1$ GPa (Jager and Fratzl, 2000) and $E_{H_2O} = 0$ GPa, are Young's moduli for the bulk phases and V_{HAP} , V_{col} and V_{H_2O} are the volume fraction of these phases. In this model, E_{HAP}^{app} has the same value as the overall composite modulus because the strain in both the HAP phase and the composite are the same. Using the experimental phase volume fractions, Eq. (2) predicts a value of 46 GPa for E_{HAP}^{app} which is significantly greater than the measured value of 26.5 ± 7.2 GPa. The difference between model and experiment may be due to biologically derived HAP having a substantially lower Young's modulus than inorganic HAP. If $E_{HAP} = 65$ GPa is used instead, the Voigt model is in agreement with the experimental apparent modulus value. Since the Voigt model is a lower limit for E_{HAP}^{app} , a HAP modulus, E_{HAP} below the above value of 65 GPa must be invoked to justify the experimental value $E_{HAP}^{app} = 26.5 \pm 7.2$ GPa. As discussed elsewhere (Deymier-Black and Almer et al., 2010), changes in HAP nano-platelet composition or crystallite size, and strain distribution effects may contribute to the difference. The presence of less load bearing HAP, for example as extrafibrillar mineral, could also cause a decrease in the apparent modulus by lowering the effective HAP volume in Eq. (2).

As mineralized fibrils represent the bulk component of dentin, it would be expected that the fibrillar modulus which represents the behavior of the fibrils would be similar in value to the ultrasonic modulus which represents the elastic behavior of the entire composite. However, the values of fibrillar apparent modulus are on average 15% lower than the ultrasonic modulus. This difference may be due to the presence of an additional, reinforcing phase in the dentin that does not contribute to the SAXS pattern. Extrafibrillar mineral, HAP mineral located outside of the collagen fibrils as described by Bonar and Lees et al. (1985) and Balooch and Habelitz et al. (2008), is a good candidate for this type of reinforcement. Without the collagen to maintain its regular spacing, the extrafibrillar HAP may not contribute to the SAXS peaks investigated here (which require ~ 67 nm periodicity); however, it still provides stiffening to the bulk sample. The 15% difference between the ultrasonic and fibrillar moduli could also simply result from experimental variations between the two techniques. Grimala and Hauperta et al. (2009) show that the ultrasonic modulus of cortical bone is systematically higher ($\sim 20\%$) than the Young's modulus

determined from three-point bending. They suggest that moduli measured by mechanical testing might provide lower values due to stress-relaxation effects. Nevertheless, the ultrasonic and fibrillar apparent moduli measured in the present study are significantly correlated ($R = 0.320$) suggesting that although their values differ, their behaviors are both dependent on similar factors, most likely the volume fraction of HAP in the sample.

4.2. Buccal–lingual spatial variations

The fibrillar and HAP apparent moduli vary significantly across a single dentin sample as shown in Fig. 5. Although no significant difference was found in the HAP or fibrillar apparent moduli between any two neighboring locations, the moduli increase in moving from the buccal edge of the sample (locations B and C) to the lingual edge (locations H and I). This difference in properties with location may be caused by a change in mineral level. The strong correlation between the location-dependent mineral content measured by μ CT and the HAP apparent modulus ($R = 0.855$), Fig. 7, suggests that variations in the HAP volume fraction plays an important role in the local variations in HAP/collagen load transfer in dentin. Three-dimensional modeling of central human incisors has shown that loading the inner crown edge at an angle of 45° (as if pulling on grass for bovine teeth, for example) will produce compressive strains on the buccal edge and tensile strains on the lingual edge (De Castro Albuquerque and De Abreu Polleto et al., 2003). Further reinforcement of the lingual edge by additional HAP may therefore have evolved to prevent excessive tensile crack propagation in the tooth structure.

Considering the strong relationship between the μ CT derived mineral content and the HAP apparent modulus, similar correlations would be expected between the TGA measurements and the apparent moduli. However, the TGA HAP fraction measurements are over volumes 250 times larger than those used in the synchrotron apparent moduli measurements, and this is most likely responsible for the lack of significant correlation between the two determinations. This interpretation is further supported by the significant correlation between the ultrasonic modulus and the TGA-determined HAP fraction which are both macroscopic measurements. Positive relationships between the volume fractions of reinforcement phases and the elastic properties in composite materials, including bones and teeth, have been shown both experimentally (Currey, 2004) and theoretically (Clyne and Withers, 1993). However, the weak correlation between these two values here ($R = 0.344$) suggests that there may be other factors at play in determining the elastic modulus of dentin which may include microstructural, histological, and biological variables.

4.3. Apical vs. cervical spatial variations

The HAP and fibrillar moduli differed for apical root dentin as compared to cervical root dentin. Here again, the difference in load transfer behavior might be related to changes in mineral content; however, the TGA did not show measurable differences between mineral content of the cervical and apical sections of the root dentin. This agrees with μ CT

measurements made by Kinney et al. (2005) which showed no difference in mineral content between the apical third, middle third, or cervical third of human root dentin. Biomechanically, the significant difference in the HAP and fibrillar moduli between the apical and cervical regions of the root may relate to the larger incisor structure of cows compared to humans. When the incisor undergoes bending upon lateral pulling (e.g., during pulling of grass), the dentin root, especially the apical tip located farthest from the crown, will be pressed against alveolar bone. It would therefore be expected that the apical section of the root would be more compliant to avoid cracking of the root tip or damage to the surrounding bone structure.

4.4. Outlook

Although this study provides significant information about how stiffness and composition vary spatially in bovine incisor root dentin, further studies focusing on increased spatial resolution are necessary. To confirm the hypothesis that the loading environment affects the distribution of properties, it will be important to establish how the properties of dentin vary along the apical–cervical direction on a much smaller length scale. Ideally, mapping the load transfer, elastic properties, and composition on a small-mesh three-dimensional grid would be necessary to completely understand variations in the elastic properties of dentin. The use of conical slits during X-ray scattering may be an option for measuring apparent moduli over small volumes within samples instead of averaging over the sample thickness; however, issues with peak broadening would have to be overcome. Although destructive, micro-indentation may be used to spatially map the elastic modulus of dentin over the entire root by testing on millimeter thick sections. Finite Element modeling of dentin might explain how the components of dentin are participating in the overall mechanical behavior of dentin and how redistribution of these components may help to protect dental integrity during physiological loading.

5. Conclusions

Various techniques (in situ high-energy WAXS and SAXS, ultrasonic velocity measurements, TGA and μ CT) applied to a population of bovine incisors provide an integrated view of root dentin's variability at the macroscopic level (via Young's modulus), sub-millimeter level (via mineral content) and nanoscopic level (via load transfer among phases). No consistent statistically significant differences in elastic properties or phase volume fractions were found between the three different types of incisors (second, third, and fourth incisor) or across five jaws from five animals. This suggests that, when performing studies where different populations of dentin are compared, it is not necessary to limit the investigation to only one type of incisor or the incisors from a single animal. It is, however, important to investigate a large population of dentin samples because intra- and inter-sample variabilities are sizable. Also, keeping a consistent sampling location among specimens (i.e., buccal vs. lingual; apical vs. cervical) is essential for valid comparisons.

Acknowledgments

The authors thank Dr. Dean Haeffner (Advanced Photon Source) and Ms. Yu-Chen Chen and Ms. Anjali Singhal (Northwestern University) for useful conversations and assistance at the beamline. This research was performed at station 1-ID-C at the Advanced Photon Source which is supported by the US Department of Energy, Office of Science, under Contract No. DE-AC02-06CH11357. ACDB acknowledges the support of the Department of Defense in the form of a National Defense Science and Engineering Graduate Fellowship, as well as the National Science Foundation in the form of a National Science Foundation Graduate Fellowship.

Appendix. Radiation dose calculation

First the sample energy absorption A_{En} was determined as:

$$A_{En} = 1 - e^{-\alpha_{En}\ell\rho} \quad (\text{A.1})$$

where α_{En} is the mass energy absorption coefficient for cortical bone at the appropriate energy (0.12 cm²/g for cortical bone at 65 keV (Hubbell and Seltzer, 1996)), ℓ is the sample thickness (0.4 cm), and ρ is the density of the sample, 1.96 g/cm³. This provides a value of $A_{En} = 0.09$. From this, the radiation dose, D , in Grays (Gy) can be calculated using the equation:

$$D = \frac{E_b \cdot \Phi \cdot t \cdot A_{En}}{M} \quad (\text{A.2})$$

where E_b is the beam energy (1.04 × 10⁻¹⁴ J for an energy of 65 keV), Φ is the flux in photons, 1.5 × 10¹⁰ ph/s, t is the exposure time, 20 s, and M is the irradiated sample mass. The irradiated sample mass of 8.23 × 10⁻⁹ kg is the product of the beam area, 30 μm × 35 μm, the sample thickness, 0.4 cm, and the sample density. The radiation dose in the present example, which is representative of samples in J1–J4, is therefore 34 kGy per scattering measurement.

REFERENCES

- Akhtar, R., Daymond, M.R., et al., 2008a. Elastic strains in antler trabecular bone determined by synchrotron X-ray diffraction. *Acta Biomater.* 4, 1677–1687.
- Akhtar, R., Daymond, M.R., et al., 2008b. Load transfer in bovine plexiform bone determined by synchrotron X-ray diffraction. *J. Mater. Res.* 23, 543–550.
- Almer, J.D., Stock, S.R., 2005. Internal strains and stresses measured in cortical bone via high-energy X-ray diffraction. *J. Struct. Biol.* 152, 14–27.
- Almer, J.D., Stock, S.R., 2007. Micromechanical response of mineral and collagen phases in bone. *J. Struct. Biol.* 157, 365–370.
- Almer, J.D., Stock, S.R., 2010. High energy X-ray scattering quantification of in situ-loading-related strain gradients spanning the dentinoenamel junction (DEJ) in bovine tooth specimens. *J. Biomech.* 43, 2294–2300.
- Avery, J.K., 1994. *Oral Development and Histology*. Theime Medical Publishers, New York, NY.
- Balooch, M., Habelitz, S., et al., 2008. Mechanical properties of mineralized collagen fibrils as influenced by demineralization. *J. Struct. Biol.* 162, 404–410.
- Balooch, G., Marshall, G.W., et al., 2004. Evaluation of a new modulus mapping technique to investigate microstructural features of human teeth. *J. Biomech.* 37, 1223–1232.
- Barth, H.D., Launey, M.E., et al., 2010. On the effect of X-ray irradiation on the deformation and fracture behavior of human cortical bone. *Bone* 46, 1475–1485.
- Bonar, L.C., Lees, S., et al., 1985. Neutron diffraction studies of collagen in fully mineralized bone. *J. Mol. Biol.* 181, 265–270.
- Clyne, T.W., Withers, P.J., 1993. *An Introduction to Metal Matrix Composites*. Cambridge University Press, Cambridge, UK.
- Craig, R.G., Peyton, F.A., 1958. Elastic and mechanical properties of human dentin. *J. Dent. Res.* 37, 710–719.
- Currey, J.D., 2002. *Bones: Structure and Mechanics*. Princeton University Press, Princeton, NJ.
- Currey, J.D., 2004. Tensile yield in compact bone is determined by strain, post-yield behaviour by mineral content. *J. Biomech.* 37, 549–556.
- Currey, J.D., Foreman, J., et al., 1997. Effects of Ionizing Radiation on the mechanical properties of human bone. *J. Orthopaed Res.* 15, 111–117.
- Daymond, M.R., Young, M.L., et al., 2007. Strain and texture evolution during mechanical loading of a crack tip in martensitic shape-memory NiTi. *Acta Mater.* 55, 3929–3942.
- De Castro Albuquerque, R., De Abreu Polleto, L.T., et al., 2003. Stress analysis of an upper central incisor restored with different posts. *J. Oral Rehabil.* 30, 936–943.
- Deymier-Black, A.C., Almer, J.D., et al., 2010. Synchrotron X-ray diffraction study of load partitioning during elastic deformation of bovine dentin. *Acta Biomater.* 6, 2172–2180.
- Deymier-Black, A.C., Almer, J.D., et al., 2011. Effect of freeze-thaw cycles on load transfer between the biomineral and collagen phases in bovine dentin. *Mater. Sci. Eng. C*. doi:10.1016/j.msec.2011.05.011.
- Fels, I.G., 1964. Hydration and density of collagen and gelatin. *J. Appl. Polym. Sci.* 8, 1813–1824.
- Gaines, R.V., Skinner, H.C.W., et al., 1997. *Dana's New Mineralogy: The System of Mineralogy of James Dwight Dana and Edward Salisbury Dana*. John Wiley & Sons, Inc., Hoboken, New Jersey.
- Gilmore, R.S., Katz, J.L., 1982. Elastic properties of apatites. *J. Mater. Sci.* 17, 1131–1141.
- Gilmore, R.S., Pollack, R.P., et al., 1969. Elastic properties of bovine dentine and enamel. *Arch. Oral Biol.* 15, 787–796.
- Grimala, Q., Hauptert, S., et al., 2009. Assessment of cortical bone elasticity and strength: mechanical testing and ultrasound provide complementary data. *Med. Eng. Phys.* 31, 1140–1147.
- Gupta, H.S., Seto, J., et al., 2006. Cooperative deformation of mineral and collagen in bone at the nanoscale. *PNAS* 103, 17741–17746.
- Gupta, H.S., Wagermaier, W., et al., 2005. Nanoscale deformation mechanisms in bone. *Nano Lett.* 5, 2108–2111.
- Gupta, H.S., Wagermaier, W., et al., 2006. Fibrillar level fracture in bone beyond the yield point. *Int. J. Fract.* 139, 425–436.
- Hammersley, A.P., 1997. FIT2D: an introduction and overview. ESRF97HA02T. ESRF Internal Report.
- Hammersley, A.P., 1998. FIT2D V9.129 reference manual V3.1. ESRF98HA01T. ESRF Internal Report.
- He, B.B., Smith, K.L., 1998. SEM spring conference on experimental and applied mechanics and experimental/numerical mechanics in electronic packaging III, Houston, TX.
- Holager, J., 1970. Thermogravimetric examination of enamel and dentin. *J. Dent. Res.* 49, 546–548.

- Hosoya, Y., Marshall, G.W., 2005. The nano-hardness and elastic modulus of sound deciduous canine dentin and young premolar dentin—preliminary study. *J. Mater. Sci. Mater. Med.* 16, 1–8.
- Hubbell, J.H., Seltzer, S.M., 1996. Tables of X-ray mass attenuation coefficients and mass energy-absorption coefficients from 1 keV to 20 MeV for elements $Z = 1$ to 92 and 48 additional substances of dosimetric interest. P.L. Ionizing Radiation Division, National Institute of Standards and Technology. <http://physics.nist.gov/PhysRefData/XrayMassCoef/cover.html>.
- Imbeni, V., Kruzic, J.J., et al., 2005. The dentin-enamel junction and the fracture of human teeth. *Nature Mater.* 4, 229–232.
- Jager, I., Fratzl, P., 2000. Mineralized collagen fibrils: a mechanical model with a staggered arrangement of mineral particles. *Biophys. J.* 79, 1737–1746.
- Kinney, J.H., Balooch, G., et al., 1996. Hardness and young's modulus of human peritubular and intertubular dentine. *Arch. Oral Biol.* 41, 9–13.
- Kinney, J.H., Gladden, J.R., et al., 2004. Resonant ultrasound spectroscopy measurements of the elastic constants of human dentin. *J. Biomech.* 37, 437–441.
- Kinney, J.H., Marshall, S.J., et al., 2003. The mechanical properties of human dentin: a critical review and re-evaluation of the dental literature. *Crit. Rev. Oral Biol. Med.* 14, 13–29.
- Kinney, J.H., Nalla, R.K., Pople, J.A., Breunig, T.M., Ritchie, R.O., 2005. Age-related transparent root dentin: mineral concentrations, crystallite size and mechanical properties. *Biomaterials* 26, 3363–3376.
- Kishen, A., Ramamurty, U., et al., 2000. Experimental studies on the nature of property gradients in the human dentine. *J. Biomed. Mater. Res.* 51, 650–659.
- Mahoney, E., Holt, A., et al., 2000. The hardness and modulus of elasticity of primary molar teeth: an ultra-micro-indentation study. *J. Dent.* 28, 589–594.
- Meredith, N., Sherriff, M., et al., 1996. Measurement of the microhardness and Young's modulus of human enamel and dentine using and indentation technique. *Arch. Oral Biol.* 41, 539–545.
- Nguyen, H., Morgan, D.A.F., et al., 2007. Sterilization of allograft bone: effects of gamma irradiation on allograft biology and biomechanics. *Cell Tissue Bank* 8, 93–105.
- Sakae, T., Mishima, H., et al., 1988. Changes in Bovine Dentin mineral with sodium hypochlorite treatment. *J. Dent. Res.* 67, 1229.
- Sano, H., Ciucchi, B., et al., 1994. Tensile properties of mineralized and demineralized human and bovine dentin. *J. Dent. Res.* 73, 1205–1211.
- Singhal, A., Deymier-Black, A.C., et al., 2011. Effect of high-energy X-rays doses on bone elastic properties and residual strains. *J. Mech. Behav. Biomed. Mater.* doi:10.1016/j.jmbbm.2011.05.035.
- Stock, S.R., 2009. *Microcomputed Tomography: Methodology and Applications*. CRC Press, Boca Raton, FL.
- Stock, S.R., Yuan, F., et al., 2011. Internal strain gradients quantified in bone under load using high-energy X-ray scattering. *J. Biomech.* 44, 291–296.
- Talmant, M., Foiret, J., et al., 2011. Guided waves in cortical bone. In: Laugier, P., Haiat, G. (Eds.), *Bone Quantitative Ultrasound*. Springer, New York.
- Ten Cate, A.R., 1980. *Oral Histology: Development, Structure and Function*. Mosby, St Louis, MI.
- Wang, R.Z., Weiner, S., 1998. Strain-structure relations in human teeth using Moire fringes. *J. Biomech.* 31, 135–141.
- Wanner, A., Dunand, D.C., 2000. Synchrotron X-ray study of bulk lattice strains in externally loaded Cu–Mo composites. *Metall. Mater. Trans. A—Phys. Metall. Mater. Sci.* 31, 2949–2962.
- Young, M.L., Almer, J.D., 2003. Diffraction measurements of load transfer in interpenetrating-phase Al₂O₃/Al composites. *Affordable Metal Matrix Composites for High-Performance Applications II*. pp. 225–233.
- Young, M.L., Almer, J.D., et al., 2007. Load partitioning between ferrite and cementite during elasto-plastic deformation of an ultrahigh-carbon steel. *Acta Mater.* 55, 1999–2011.
- Young, M.L., DeFouw, J.D., et al., 2007. Load partitioning during compressive loading of a Mg/MgB₂ composite. *Acta Mater.* 55, 3467–3478.